International Journal of Environmental Sciences
ISSN: 2229-7359
Vol. 11 No. 23s, 2025
https://theaspd.com/index.php

Various Ceramic-Based Coatings on High-Speed Steel (HSS) Substrate: Mechanical and Tribological Properties

Anish Kumar Bisht[1], Rahul O Vaishya[2*], Rajesh Kumar Chandel[3], Ramandeep Singh[4*], Jimmy karloopia[5], Amarjeet Kumar[6]
[1,2*,3,4*,5,6]Department of Production and Industrial Engineering, Punjab Engineering College (Deemed to be University), Chandigarh, 160012, India
anishbisht1992@gmail.com[1], rahulvaishya@pec.edu.in[Z*], rkchandel156@gmail.com[3], ramandeepsingh.phd23prod@pec.edu.in[4*], jimmykarloopia@pec.edu.in[5], amarjeet.kumar714@gmail.com[6]

***Corresponding Author:** Rahul O Vaishya
Email: rahulvaishya@pec.edu.in, ramandeepsingh.phd23prod@pec.edu.in

Abstract
In modern times, tribology plays a significant role in energy degradation, primarily due to friction, which leads to substantial energy loss and material degradation. Coating is a highly viable technique to reduce this impact. In this paper, ceramic-based coatings, specifically oxide and non-oxide types, are considered for mechanical and tribological use with a high-speed steel (HSS) substrate. Ceramic coatings are vital to HSS cutting tools from mechanical and tribological damage. A comprehensive surface morphology of coatings and mechanical and tribological properties, such as hardness, elastic modulus, surface roughness, wear rate, and coefficient of friction, are thoroughly investigated. The findings indicate that ceramic-based coatings significantly enhance the lifespan and efficiency of HSS tools, making them indispensable in high-performance machining and cutting tool industries.
Keywords: *Coatings; High-speed steel; Tribological and mechanical properties; Ceramics; Cutting tools.*

1. INTRODUCTION

High-speed steels comprise a group of alloys used for cutting tools. The two characteristics listed below are combined to form their name, high-speed steel (a) These alloys are part of the Fe–C–X multicomponent system, where X denotes a group of alloying elements primarily Cr, W or Mo, V, and Co (b) They are characterized by their ability to retain high hardness even at elevated temperatures generated during high-speed metal cutting [1–3]. HSS tools are crucial in cutting operations due to their working ability to withstand high temperatures without losing their hardness (63–68 HRC), thereby allowing for faster cutting speeds (higher than 30 m/min) when compared to traditional steels. This makes them well-suited for a wide range of machining applications that demand durability and high performance, including characteristics such as: (i) good wear resistance, (ii) ability to be reground, and (iii) cost-effectiveness, making them a popular choice for various cutting tools like (i) drills, (ii) taps, and (iii) milling cutters. High-speed steel offers high hardness, wear resistance, good toughness, and good fracture resistance i.e. toughness, making it suitable for cutting tools with high rake angles, and machine tools prone to vibrations [4,5]. Due to the continuous use of HSS at high temperatures, high contact pressures, and a rise in wear rate is imminent as a result of severe chemical reactions [6–8]. Therefore, to increase the wear resistance of the cutting tool, coating enhances the tool life [9]. Various types of coatings are widely used that result in an enhancement in the material properties. Additionally, coating layers can reduce cost, while neglecting the scarcity of the materials, as the coatings are a few micrometers thick [10]. The coatings can provide a range of benefits, including the factor:(i) improved resistance to corrosion and wear, (ii) increased surface durability, (iii) customized surface finishes, (iv) thermal and electrical insulation, (v) modified fluid dynamics, (vi) hydrophobicity, and much [11]. In cutting tool industries, tool steels are mainly classified as M-type and T-type based on the use of molybdenum or tungsten as the primary alloying element. A shortage of tungsten (W) led to the finding of molybdenum (Mo) as a stable substitute. Tool steels (T and M) are nearly identical and provide the same properties while having comparable cutting performance. Generally, the M-type tool steels are more widely used and less expensive (≅30%) and popular (≅85% of all tool steels) and when compared to the T-type counterparts. Various surface treatment methods are available for HSS tools, concentrated to the following: (i) physical vapour deposition (PVD), (ii) chemical vapour deposition (CVD), (iii) thermal spray coating, (iv) thermal diffusion, (v) boronizing [12–19]. In the early days, CVD with high-temperature deposition (950-1050 °C) was used. As a result, there is an embrittlement of the coating edge, especially if a significant amount of

the brittle eta phase is formed when found near the substrate coating interface. Another limitation is the higher thickness of the coating. As a result, the adhesion strength drops drastically. Despite the issue as mentioned above, most of the carbide inserts remain coated using the chemical vapour deposition technique. So to overcome this problem, the PVD process has been used when the deposition temperature is about 500 °C. Therefore, the most common coating method used on a HSS tool is sputtering, physical vapor deposition (PVD) [20]. In recent years, thermal spray coatings are also used for HSS tools. The coating on HSS cutting tools provide a hard, wear-resistant layer, which is essential for extending the lifespan of the working and enhancing their functionality [21]. In this review article, the authors finding that ceramic-based coatings are preferred for improving the tribological and mechanical properties of substrates at high temperatures, offering properties like (i) high stability, (ii) hardness, (iii) good wear and corrosion resistance [22]. Owing to their excellent resistance to harsh operating conditions, these coatings have been extensively applied to enhance the longevity of gas turbines, aerospace components, and high-speed cutting tools [20,22].

Table 1. Shows the coating characteristics for PVD, CVD, and thermal spray coating.

S. No	Coating Process	Coating Thickness	Temperature	Deposition rate	Wear resistance
1	PVD	1-5 μm	200-500 °C	1-10 nm/s	Low
2	CVD	1-50 μm	500-1200 °C	1-10 μm/hr	Moderate
3	Thermal spray coating	0.04-3 mm	>1200 °C	Several grams per second	High

Table 1 shows three advanced coating techniques: (i) PVD, (ii) CVD (iii) Thermal spray coating based on deposition characteristics and wear resistance. PVD produces thin, dense coatings at low temperatures, which is ideal for precision tools but offers limited wear resistance [23,24]. CVD, operating at higher temperatures, enables thicker coatings having adhesion and hardness but can introduce thermal stress, thereby limiting its application on temperature-sensitive substrates [25]. Thermal spray coatings provide the thickest deposits and excellent wear and corrosion resistance; therefore, adhesion is primarily mechanical, leading to potential delamination under the influence of external load [26].

2. Ceramic coatings on HSS for Tribological/Mechanical applications

Numerous researchers examined the various coatings, i.e. nitride, carbide, and oxide base ceramic coatings, include binary, ternary, and multielemental, which improve the tribological performance of various substrates [27]. Currently, researchers focus on advanced materials like ceramics, bio-ceramics, carbon nanotubes (CNT) [28], diamond-like carbon (DLC) [29,30], and hybrid coatings [28] due to their (i) superior hardness, (ii) corrosion resistance, (iii) wear resistance, and (iv) self-lubricating properties. Hard protective layers in ceramic form, comprising borides, oxides, sulphides, nitrides, and carbides, exhibit superior durability and corrosion resistance [31]. Generally, desirable tribological properties and mechanical properties including the following (i) high values of hardness (H), (ii) Young's modulus (E), $\frac{H}{E}$ and $\frac{H^3}{E^2}$ Ratios, (iii) greater adhesion strength, (iv) low coefficient of friction (COF), and (v) less wear rates required for working [32,33].

Numerous research papers are available on the fundamentals of tribology and conventional ceramic coatings for tribological usage [34–37]. But in this review article, the author summarises the fruitful findings, i.e., hardness, coefficient of friction, wear rate, corrosion resistance, etc., to conclude ceramic coatings on high-speed steel (HSS).

Mechanical and tribological properties of various ceramic-based coatings on HSS.

2.1.1 TiB_2-Al_2O_3-Ti(20%) coating on HSS

Ahmad et al. examined the effect of the TiB_2-Al_2O_3-Ti(20%) coating using the electron beam deposition method on high-speed steel, with an emphasis on (i) microstructure, (ii) hardness, (iii) surface morphology, (iv) adhesion wear, and (v) crystallographic roughness [38]. The main function of Al_2O_3 is to improve the high hardness value, stability at high temperatures, protection from oxidation, and good elastic modulus [39]. In this type of coating, Ti enhances adhesion strength between the coating and the substrate while also increasing the elastic modulus [40,41]. The nano-hardness and Young's modulus of TiB_2-Al_2O_3-Ti(20%) coating and uncoated substrate were examined using five peak loads ranging from

2000 µN to 10000 µN. Nano-scratch tests were conducted on the coated substrate with loads ranging from 0 to 10,000 µN to assess the adhesion strength of coatings. The 2D and 3D indentation images of the TiB_2-Al_2O_3-Ti(20%) coating were obtained using an Atomic Force Microscope (AFM) at a minimum load of 2000 µN (Fig. 1. (a,b)). The TiB_2-Al_2O_3-Ti(20%) coating did not assemble near the indent mark, indicating that the TiB_2-Al_2O_3-Ti(20%) coating is a hard material. A similar pattern was observed at loads ranging from 4000 µN to 10,000 µN, as shown in Fig. 1(c-j). The uncoated HSS sample exhibits a certain level of behavior shown in Fig. 2. However, the HSS findings reveal less flexibility and hardness in comparison to the coated sample.

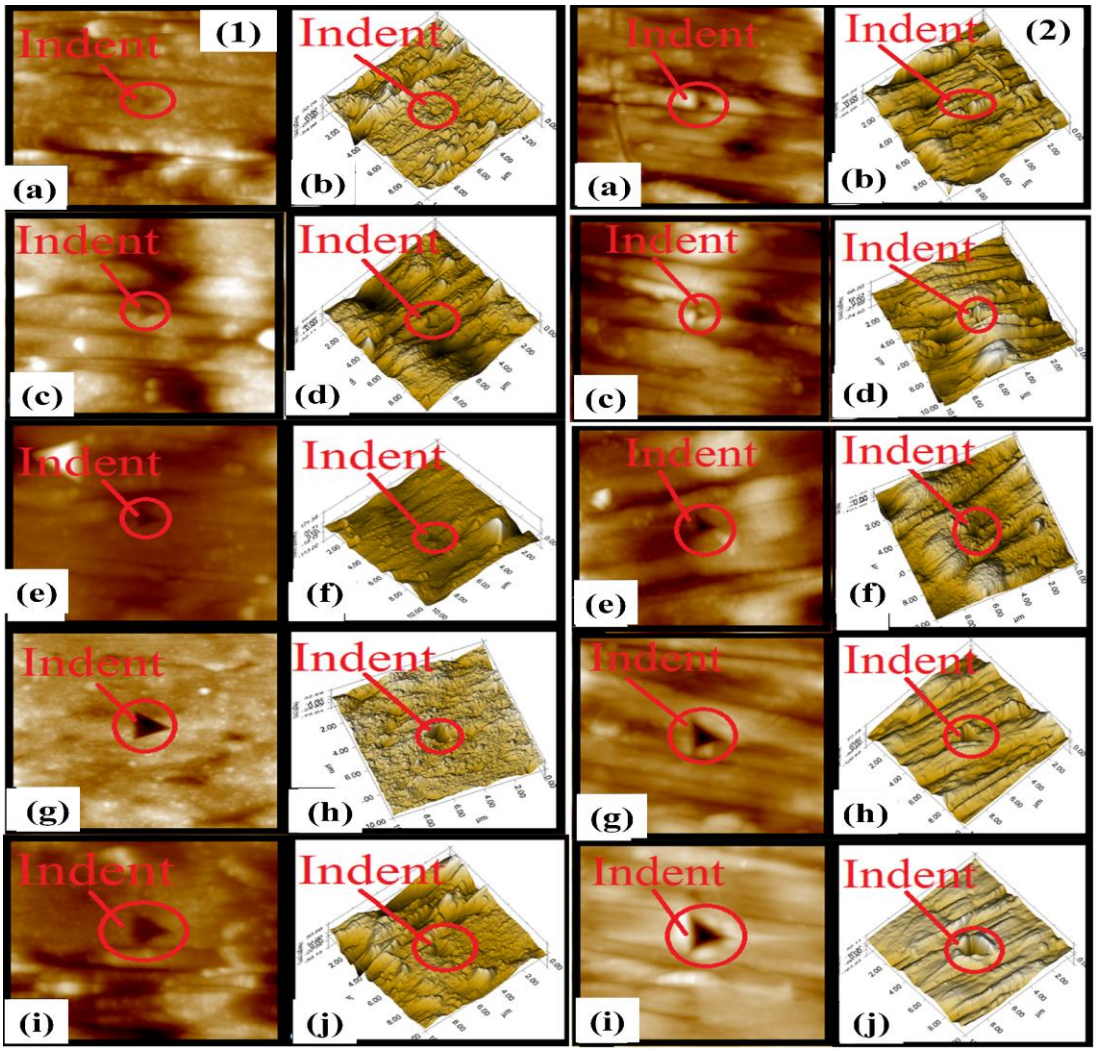

Fig. 1 and 2: Fig. 1 shows the 2D and 3D images of coated samples indented under varying loads; (a-b) at a load of 2×10^{-3}N, (c-d) at a load of 4×10^{-3}N, (e-f) at a load of 6×10^{-3}N, (g-h) at a load of 8×10^{-3}N, and (i-j) at a load of 1×10^{-3}N. Fig. 2 shows the 2D and 3D images of uncoated HSS samples indented at the same load corresponding [38]**.**

Titanium nitride (TiN) coating on HSS

Tillmann et al. deposited TiAlN, TiAlSiN, and TiAlTaN-based thin film coatings on microend mills using a customized PVD method [42]. The researchers used different coating techniques (i) magnetron spectrum (MS) [43], (ii) direct current magnetron sputtering (dcMS), and (iii) hybrid dcMS/HiPIMS [44] on micro milling cutters as a substrate. The Hybrid dcMS/HiPIMS provides improved tribological and mechanical properties than the other two methods [45,46]. SEM morphology of the thin film of the coating on a flat cylindrical HSS substrate and the initial state of coated micro end mills as shown in Fig. 3. All direct current magnetron sputtering (dcMS) thin films display a columnar-like structure, whereas the TiAlSiN coating using direct current magnetron sputtering (dcMS) exhibits a more denser morphology. In contrast, dcMS/HiPIMS-TiAlN and dcMS/HiPIMS-TiAlTaN possess dense structures with minimal columnar-like features.

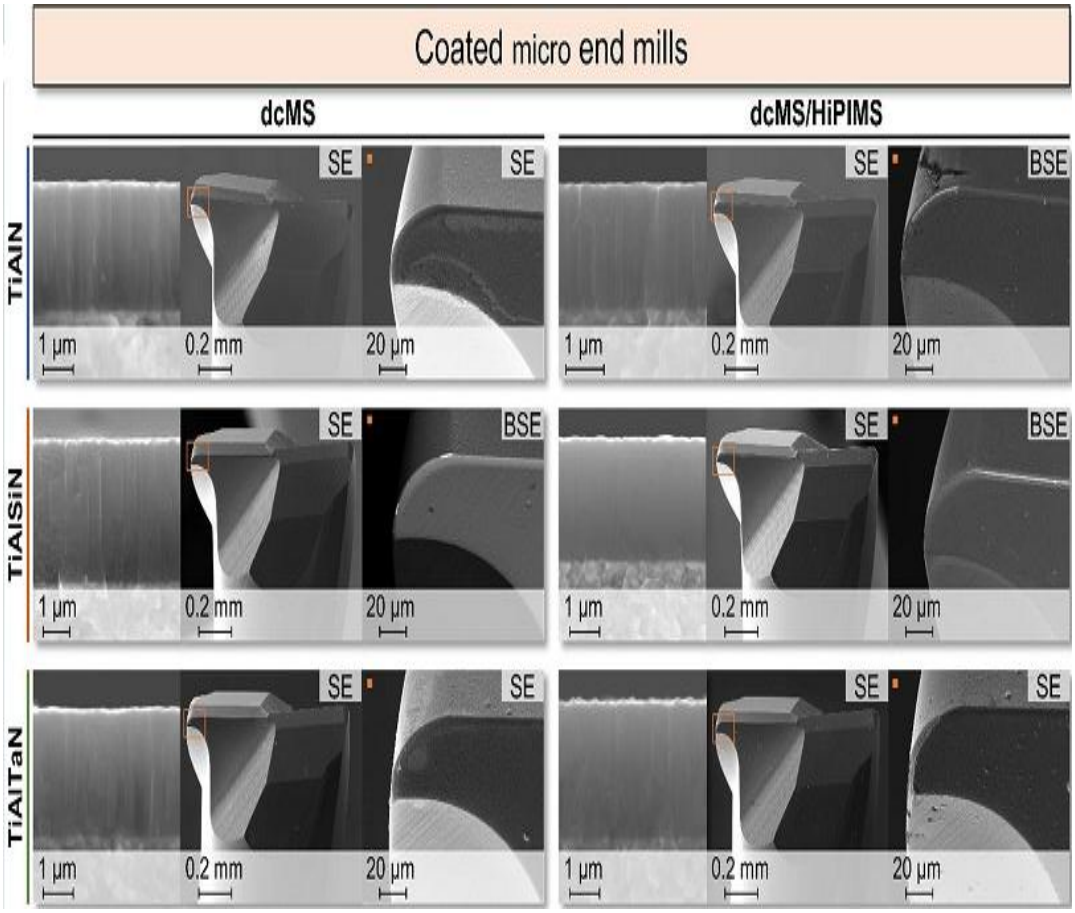

Fig. 3. SEM image of TiAlN, TiAlSiN, and TiAlTaN coating deposited by either dcMS or dcMS/HiPIMS [42].

2.1.3 Characteristics and wear performance of TiN, TiAlN, CrN, AlTiN, and TiCN coating on M41 HSS using the PVD technique.

Ozgur et al. [47] examined the thermal characteristics and wear performance of ceramic-based coatings applied using arc physical vapor deposition (Arc PVD) technology on M41 high-speed steel. More specifically, they aimed to compare five different coatings - TiN, TiAlN, CrN, AlTiN, and TiCN in terms of microhardness, wear resistance, and thermal diffusivity, thereby identifying the most promising coating for applications where both abrasive loading and high temperatures are enhanced [47]. To achieve this, the M41 was used as the substrate. Fig. 4(a) shows a schematic representation of heat flux in a cutting tool, illustrating that friction between the workpiece (or chip) and the tool generates significant localized heating at the tool tip. The highest temperature occurs near the high-pressure and friction zone, which is precisely where the tool material is most vulnerable to accelerated wear. By mapping out this zone of critical heat flux, Fig. 4 reveals that both wear and temperature rise are strongly interlinked. Thus, materials or coatings with appropriate thermal properties can help moderate the localized heating and extend tool life [47]. The microhardness values of the various PVD coatings compared to the uncoated M41 steel as shown in Fig. 4(b). CrN exhibits a hardness near 2400 HV, TiN around 3100 HV, TiCN and TiAlN each about 3300 HV, and with AlTiN reaching the highest value (approximately 3800 HV). By contrast, the uncoated M41 substrate registers around a hardness of 850 HV. The researchers have observed that coatings with higher hardness generally provide better protection against abrasive wear [47]. Comparison of total mass loss (%) (Fig. 4(c)) for the coated samples after 8000 m of sliding wear. AlTiN and TiAlN demonstrate the lowest mass loss (˜0.075% and ˜0.085%, respectively), indicating superior wear resistance. The TiN follows close behind, whereas TiCN and CrN incur noticeably higher mass losses, the TiCN around 0.110% and CrN around 0.150%, showing that they are comparatively less effective against abrasive wear under the test conditions. Fig. 4(d) reveals the variation in thermal diffusivity for each coating as the temperature increases from room temperature to 800°C. All the coatings exhibit a modest increase in diffusivity up to roughly 300–350°C, followed by a decline as temperatures continue to climb. Notably, the CrN and TiN maintain higher diffusivity values than the bare M41 steel

substrate across much of the temperature range, whereas the TiAlN and AlTiN remain below those of the uncoated steel [47].

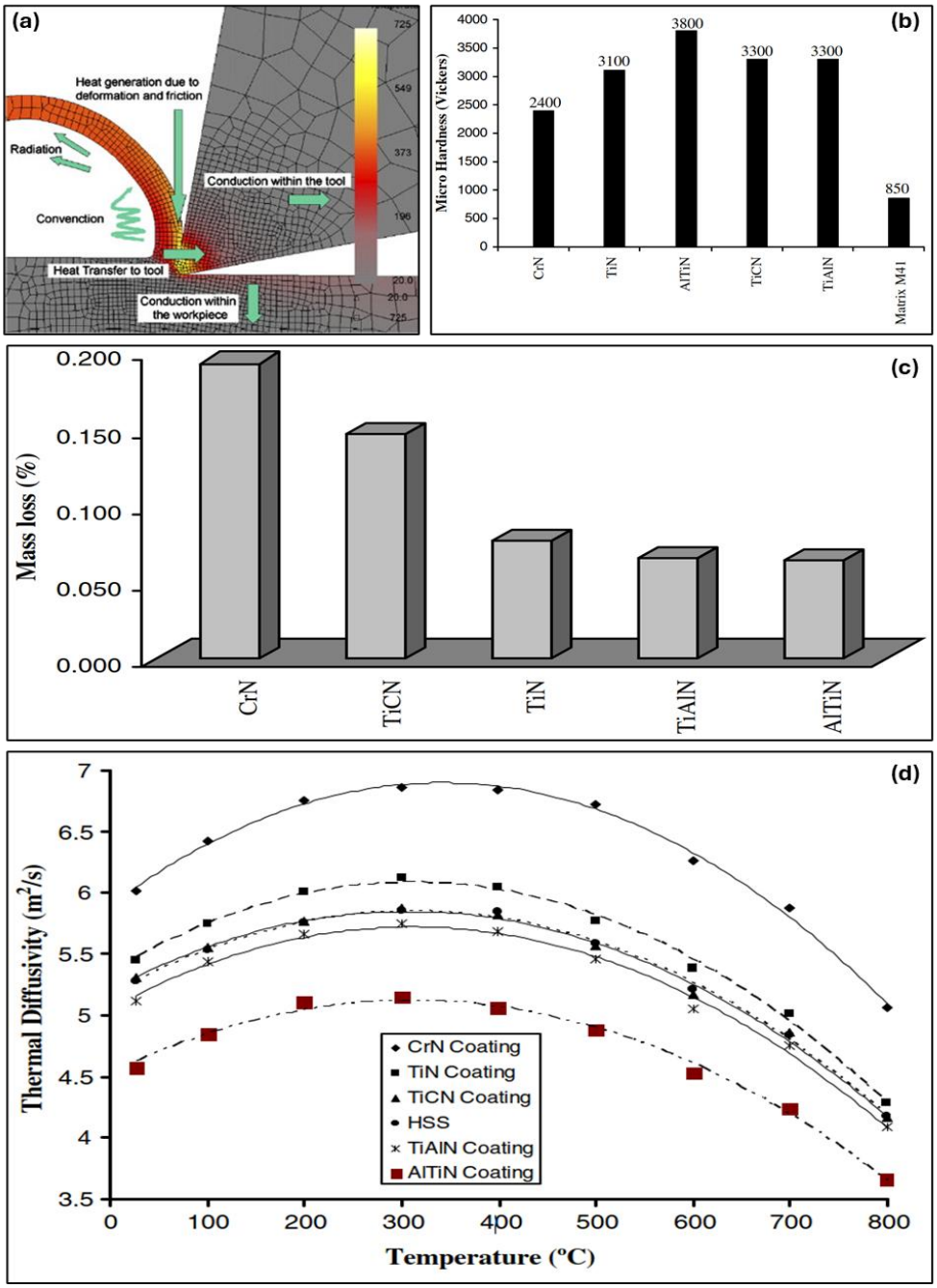

Fig. 4. (a) Illustrating the distribution of thermal energy flow throughout the cutting tool's structure [48]; (b) measured micro-hardness values for the surface coatings; (c) The overall variations in mass loss for the coated samples were evaluated over a wear distance of 8000 m; (d) The coated samples exhibit a marked dependency of thermal diffusivity on temperature changes [47].

2.1.4 Diamond-Like Carbon (DLC) coating

Vieira et al. deposited diamond-like carbon (DLC) coatings that have low coefficient of friction, high hardness, and chemical resistance characteristics that can improve the performance of mechanical components and cutting tools [49]. Several types of diamond-like carbon (DLC) films are known, include (i) hydrogenated tetrahedral amorphous carbon (ta-C:H), (ii) hydrogenated amorphous carbon (a-C: H), (iii) tetrahedral amorphous carbon (ta-C), and (iv) amorphous carbon (a-C) films. To increase adhesion, a chromium interlayer deposition was done before the diamond-like carbon (DLC) film was deposited. The solid graphite electrode used for the coating was composed entirely of carbon (about 99 percent). In this process, the film condenses from an ion beam, which impacts the substrate and induces sp^3 bonds during growth. The coating is identified from the surface to an average depth of 1.5 μm, exhibiting a uniform, crack-free, and void-free deposition as shown in Fig. 5.

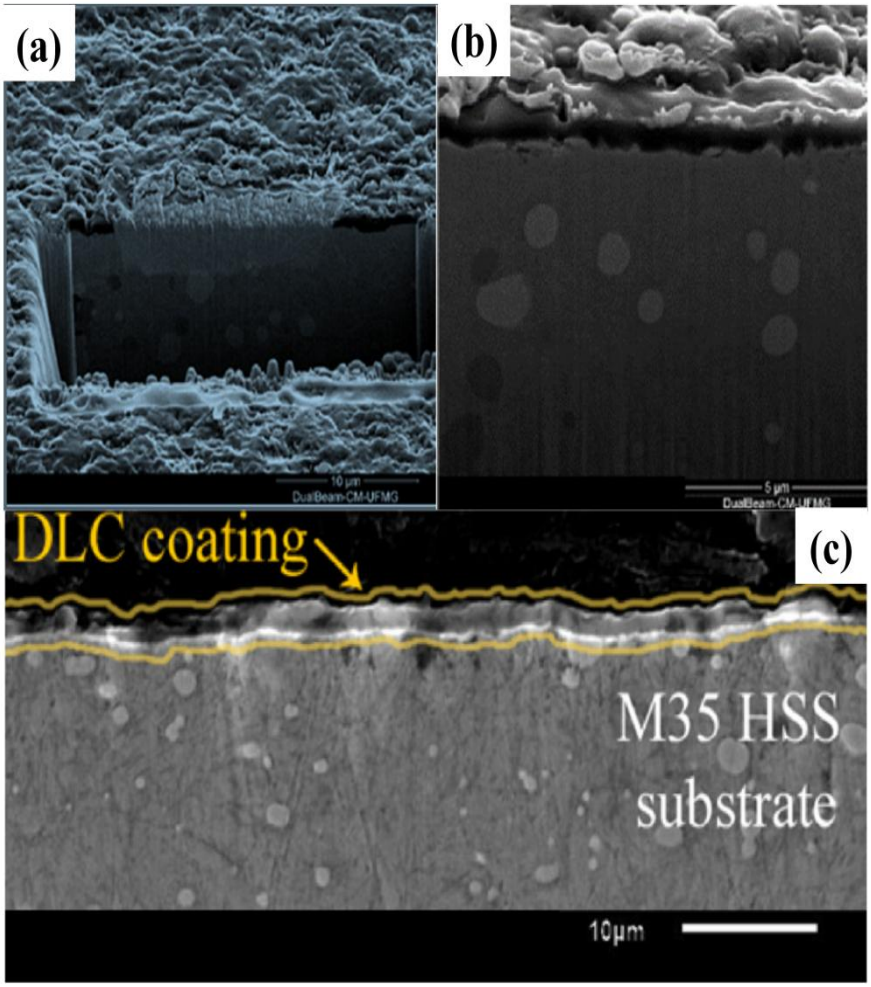

Fig. 5. SEM image of the diamond-like carbon (DLC) deposition on M35 HSS (a) Cut section of diamond-like carbon (DLC) coating (b) Section magnification (c) Diamond-like carbon (DLC) film region evaluated [49].

2.1.5 B-C-N diffusion coating on HSS

Chaus et al. [50] analyse the chemical characteristics and microstructure of the steel after undergoing complete heat treatment, as shown in Fig. 6. Two different kinds of carbides with chemical compositions that match the M_6C and MC phases are found in a martensitic matrix (Fig. 6 (c) and Fig. 6(d), respectively). A detailed characterization of the different carbide morphologies observed in AISI M2 tool steel, based on elemental composition and microstructural features by Choudhari et al. [51] as shown in Fig. 6(e). The study identifies three primary carbide types: M_6C, MC, and M_2C, along with their respective weight percentages of molybdenum (Mo), tungsten (W), chromium (Cr), iron (Fe), and vanadium (V) determined through energy dispersive X-ray spectroscopy (EDS). The M_6C carbide phase, rich in tungsten and molybdenum, exhibits distinct morphological features such as fishbone-like, rod-like, or spider-web-shaped structures. The MC carbide phase primarily comprises vanadium, exhibiting a fan-like morphology. These carbides contribute to hardness and wear resistance due to their high V content (46.56%), along with moderate concentrations of W (25%) and Mo (18.73%). Iron (Fe) in MC carbides is significantly lower than M_6C, thereby suggesting that these carbides are more stable in high-alloy tool steels and play a critical role in strengthening the matrix. The metastable M_2C carbide phase was detected predominantly in the furnace-cooled samples sintered at 1270 °C, but it decomposes into stable M_6C and MC phases at higher sintering temperatures of 1280 °C and 1300 °C. The M_2C carbides exhibited the highest tungsten (~42%) and molybdenum (~30%) content, with minimal Fe, Cr, and V. The study concludes that microstructural evolution of the AISI M2 tool steel is significantly influenced by the carbide distribution and morphology, thereby affecting mechanical properties such as (i) hardness, (ii) wear resistance, and (iii) toughness etc.

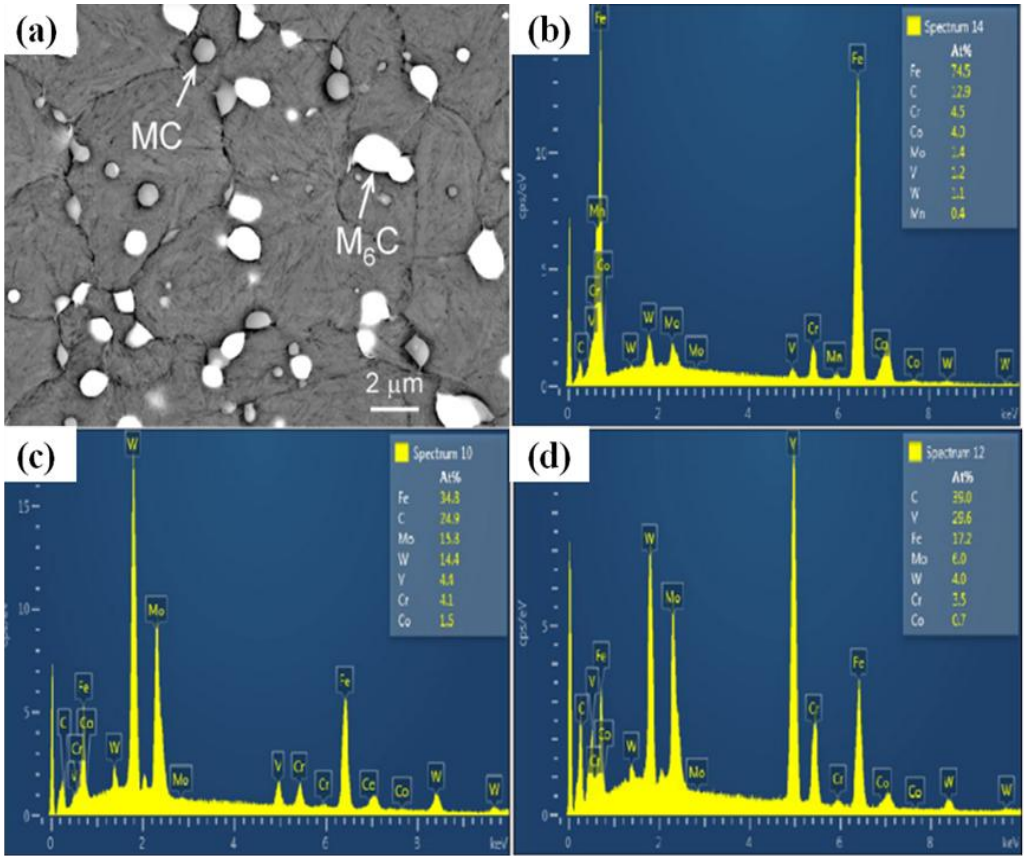

(e)

Carbides	SEM\EDS image	Elements (%)	1	2	3	4	5	Average (%)	Structure	Shapes
M_6C	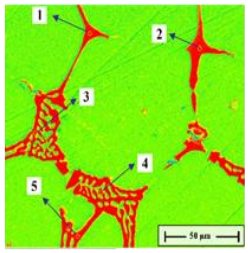	W	37.13	36.33	38.21	38.16	38.31	37.62 ± 2	FCC	Fishbone Rode like Spider webs
		Mo	26.02	27.71	24.5	24.45	24.01	25.33 ± 2		
		V	3.30	3.19	3.91	4.03	3.84	3.65 ± 0.5		
		Cr	3.59	3.64	3.44	3.49	3.41	3.52 ± 0.5		
		Fe	29.96	29.14	29.94	29.88	30.43	29.87 ± 3		
MC	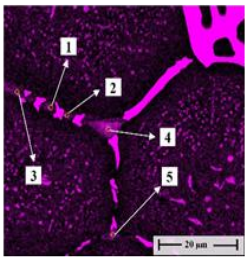	W	24.5	24.81	25.22	24.72	24.12	25.00 ± 2	FCC	Fan Shape
		Mo	18.92	18.61	19.22	18.99	19.08	18.73 ± 2		
		V	46.59	47.48	48.13	45.62	46.33	46.56 ± 3		
		Cr	3.88	3.72	3.44	3.94	4.2	3.96 ± 0.5		
		Fe	6.11	5.38	3.99	6.73	6.27	5.74 ± 1		

Fig. 6. (a) Surface morphology of M35 HSS after complete heat treatment and EDS patterns for (b) carbides and matrix (c) M_6C, and (d) MC [50], (e) characteristics of different carbide types in AISI M2 tool steel.

2.2 Tribological properties of ceramic-based coatings on HSS

2.2.1 Tribological properties of TiB_2-Al_2O_3-Ti(20%) coating

Ahmad et al. [38] carried out nanowear tests for a total of 15.91 minutes at a speed of 30 rpm on the coated and untreated surfaces. The time vs coefficient of friction of the coated sample and uncoated HSS samples are shown in Fig. 7(a) and (b). When compared to an uncoated HSS sample, the coated sample's wear mechanism is primarily ductile, and the abrasive wear mechanism results in a consistent and low frictional coefficient. The coated HSS sample exhibited a lubricating effect with a friction coefficient between 0.08 and 0.17, whereas the uncoated HSS displayed a higher friction coefficient of 0.1 to 0.58 due to adhesive wear [38].

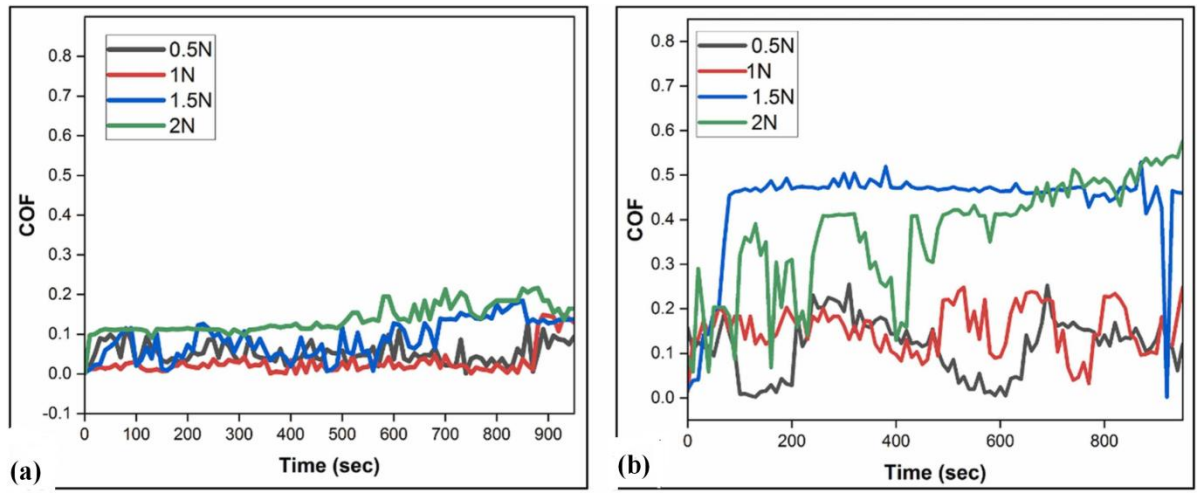

Fig. 7. Variation of graph between Time vs COF with (a) TiB_2-Al_2O_3-Ti(20 %) coating on HSS and (b) uncoated HSS substrate [38].

2.2.2 Tribological properties of diamond-like carbon (DLC) coating

Vieira et al**.** [49] conducted a tribotest to ascertain the tribological pair's coefficient of friction, which was 0.10, as determined by the pin-on-disc (POD) test and sliding wear test experiment, as shown in Fig. 8(a). The generated model is shown in Fig. 8(b), where the interlayer and thin film thicknesses were preserved. More aggressive outcomes in the areas of interest were obtained for both bodies by refining the triangular mesh was applied to the areas that were in contact with the surroundings as shown in Fig. 8(c). Finally, simulations were conducted using various tip radii of (i)0 nm, (ii)100 nm, (iii)150 nm, (iv)175 nm, (v)215 nm, (vi)225 nm, and (vii)250 nm for the partial indentation test [49].

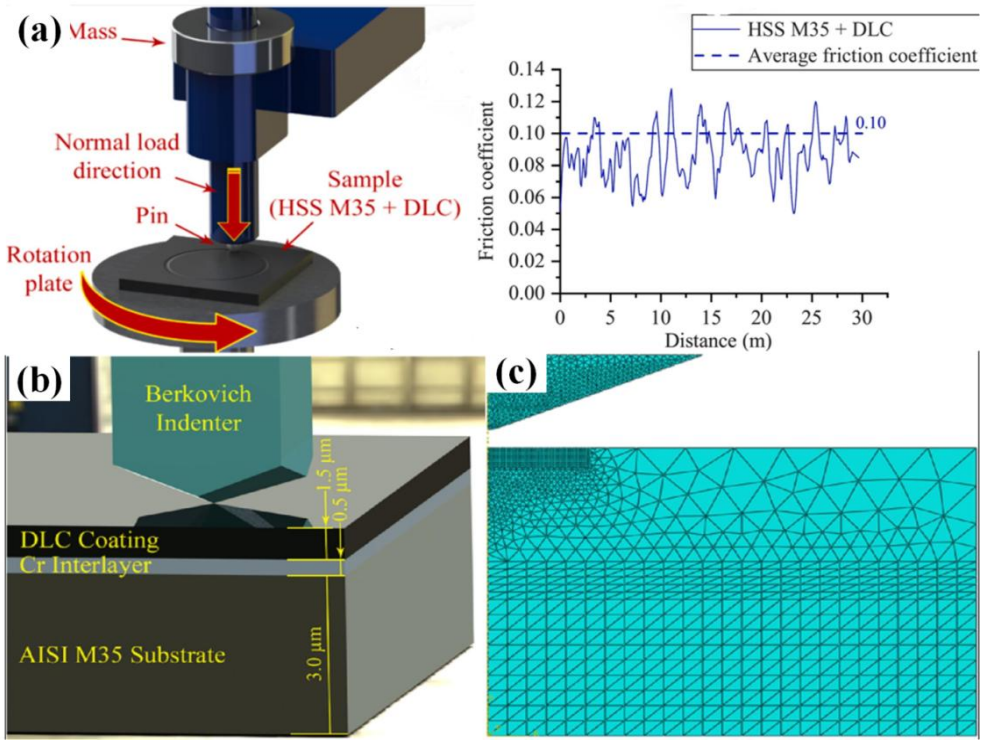

Fig. 8. (a) Pin-on-disc test for tribological study (b) nanoindentation model synthesis (c) finite element meshing (FEM) generated [49].

2.2.3 Tribological properties of TiB_2/TiC multilayer coatings by magnetron sputtering (MS)

Lee et al. [52] showed that the progression of wear volume for different coatings with increasing sliding time is shown in Fig. 9. Because of its high hardness (60 GPa), the 3:0.5 multilayer coating, that is, a layer thickness of 3.0 nm for TiB_2 and 0.5 nm for TiC, was selected for this investigation. On comparing the multilayer to monolithic TiB_2 and TiC coatings, Fig. 9 shows that the multilayer provides better wear resistance. The tool steel is not much protected from wear by the monolithic TiC coating. Conversely, the multilayer coating enhances wear resistance by a factor of four compared to the uncoated M2 steel substrate after a 10-minute sliding test [52].

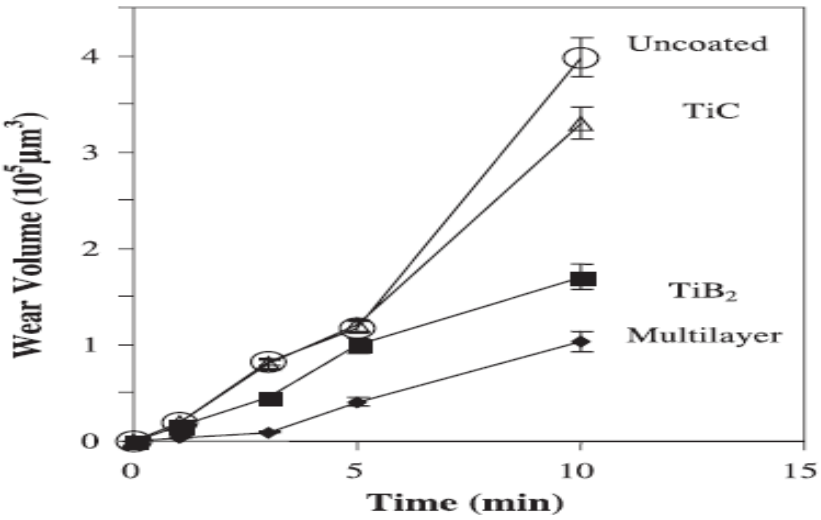

Fig. 9. Graph between the wear volume of different coatings vs sliding time. All experiments were conducted under dry sliding conditions using the block-on-ring configuration, having linear sliding speed of 0.139 m/s and a normal load of 75 gm [52].

Table 2. Ceramic-based coating on high-speed steel (HSS) for Mechanical/Tribological properties.

Author [Ref.] (Year)	Coating Material	Method	Coating Thickness (µm)	Wear Resistance/ Wear rate	COF	Hardness	Remarks
Wanstrand et al. [53] (1999)	WC/C	PVD	2 and 4	155±14 to 313±33 mm^3/ Nm	~	1500 and 1800 HV	• The coating exhibits the lowest wear rate among the counter materials.
Zheng et al. [54] (2010)	CN_x/TiN	Pulsed laser	For CN_x: 25, 33, 42 nm For TiN: 28, 21, 12 nm	2.5 ×10−7m m^3 /Nm	For bilayers: (1-10 nm) 0.11–0.14	30 GPa	• When the CN_x to bilayer thickness ratio is increased, the multilayer film's hardness, friction coefficient, and wear rate all decrease.
Panich et al.[55] (2010)	TIB_2	DCMS and RFMS	1.85, 1.7, 3.15, 1.75, 2.9 µm	Improved by three times	At steady state: 0.65	44.1 GPa	• Coatings improve the wear resistance about three times.
Warcholinski et al. [56](2010)	CrCN/CrN	CAE-PVD	400 nm	Wear rate is 4 times lower than the substrate.	COF reduced by 20%	25± 3 GPa	• Low carbon addition at 10% decreased COF, wear rate, and hardness compared to chromium

							nitride without carbon content.
Tillmann et al. [57] (2012)	TiBCN	DCMS	2 μm	$0.744\times10^{-7}mm^3/Nm$	0.82 to 0.99	34.3 GPa	• Wear rate of the sample deposited using a 60 sccm N_2 flow was 4 times lower than the uncoated sample.
Sahab et al. [58] (2012)	Al_2O_3 3%wt TiO_2	Plasma Spray Coating	~	~	For sample (S6), Min. 0.678 ± 0.038 to For sample (S7), Max. 0.801 ± 0.049	At SOD (75 mm): 473.1 to 736.7 Hv At SOD (90 mm): 587 to 772.7 Hv	• Increasing the SOD from 75 mm to 90mm led to improved hardness performance and the lowest COF encountered.
Ravi et al. [59] (2015)	TiN and Ti–Al–Si–N	CAE-PVD	2 μm	~	~	For TiN: 24 HV For Ti–Al–Si–N: 40 HV	• Compared to nanocomposite, TiN coating adheres to the substrate better at low surface roughness (R_a<0.03), but they become nearer at higher surface roughness (R_a>0.03).
Vieira et al. [49] (2017)	DLC	PVD	0.5 to 5 μm	~	0.01 and 0.25	9.25 ± 2.10 GPa	• Modifying the indenter tip radius had a minimal effect on indentation force and material hardness results.
Chaus et. al. [50] (2017)	B-C-N	Diffusion coating	~	~	~	225 HB	• Coated drill tool life improved by approximately 120% compared to

							uncoated drill performance.
Mughal et al. [60] (2018)	Nano-composite ceramic coatings (nc-AlTiN/a-Si_3N_4)	PVD	2.5- 4 µm	Flank wear: 20, 80, 160, 180 µm	~	100 HV	• Maximum improvement in tribological performance occurred at a 4µm coating thickness with a 34% average increase relative to the baseline TiN.
Kuo et al. [61] (2019)	TiN	HiPIMS, DCMS	2.4and 2.5 µm	~	~	1568 and 1277 $HV_{0.1gf}$	• Titanium nitride (TiN) coating deposited by HiPIMS exhibits better mechanical properties and exceptional wear resistance at high temperatures (300 °C).
Manivannan et al. [62] (2020)	Al_2O_3, SiC and B_4C	Sputtering and thermal evaporation	1.1-1.9 µm	Flank wear: 20-24 µm	0.371-0.452	37.2 GPa	• The lifespan of coated HSS tools increased sevenfold compared to uncoated tools.
Ali and Nazar [38] (2022)	TiB_2/ Al_2O_3	EB-PVD	1.276–1.367 µm	2.6808×10^{-3} to 4.461×10^{-3} mm^3/m	0.08 to 0.17	24 to 33.93 GPa	• In comparison to the underlying material, the coated surface has a lower coefficient of friction.
Daniel et al. [63] (2023)	CoCrW/ CoCrAlYTaCSi	HVOF	400 µm	~	~	For CoCrW 7.1 ± 0.8 GPa For CoCrAlYTaCSi: 10.4 ± 0.6 GPa	• For HVOF sprayed Co-based coatings, sliding/abrasive wear results do not match to dynamic impact wear.
Midab et al. [64] (2023)	Titania and alumina	Sol-gel	For monolithic:	~	~	~	• A multilayer of alumina/titania exhibited a

			2.707, 6.165, 11.6 μm For twolayers: 3.666, 5.027, 17.006, 22.985 μm				maximum adhesive strength of 89MPa at a 30-second immersion time.
Kumar et al. [65] (2024)	Al_2O_3–13% TiO_2	D-Gun	212 and 196 μm	Wear resistance improved by 36.25%	~	251-334 HV	• In comparison to coated samples before cryogenic treatment (CBCT) and uncoated samples, there was a 54.05% and 36.25% abrasion loss.
Lin et al. [66] (2024)	TiAlSiN	HiPIMS	2.5-4 μm	Wear resistance enhanced by 58.6%.	0.62-0.7	19-26.55 HV	• Enhanced tribological and mechanical properties, including increased wear resistance and hardness.
Pereira et al. [67] (2024)	SiO_2	Sol–gel	490 to 550 nm	~	For SiO_2: COF Reduces up to 55% For TiN: Reduce up to 63%.	For SiO_2: 1.8-4.7 GPa For TiN: 35-45 GPa	• SiO_2 coating exhibited some limitations forsliding speeds higher than 55 $mmin^{-1}$.
Bobzin et al. [68] (2024)	TiAlCrSiN	HiPIMS and DCMS	~	~	Apparent COF ≅1.5	~	• Coatings like TiAlCrSiN/TiAlCrSiN have great potential to reduce material sticking to tool surfaces and thereby improve tool performance.

Martins et al. [69] (2025)	DLC	PVD sputtering	683-782.7 nm	Without DLC: $2.04\times10^{-5}mm^3/Nm$ With DLC: $1.44\times10^{-7}mm^3/Nm$	Improved by ~ 42%	• Abrasion wear was reduced by 71% compared to uncoated samples.

Table 3. Nomenclature

HiPIMS	high power impulse magnetron sputtering
RFMS	radio frequency magnetron sputtering
MOCVD	metallo-organic chemical vapour deposition
CAE- PVD	cathodic arc evaporation physical vapour deposition
RFMS	radio frequency magnetron sputtering
EB-PVD	electron beam physical vapour deposition
DCMS	direct current magnetron sputtering
MS	magnetron sputtering
COF	coefficient of friction
PVD	physical vapour deposition
CVD	chemical vapour deposition
HVOF	high velocity oxy fuel
HSS	high-speed steel
DLC	diamond-like carbon
SOD	stand of distance

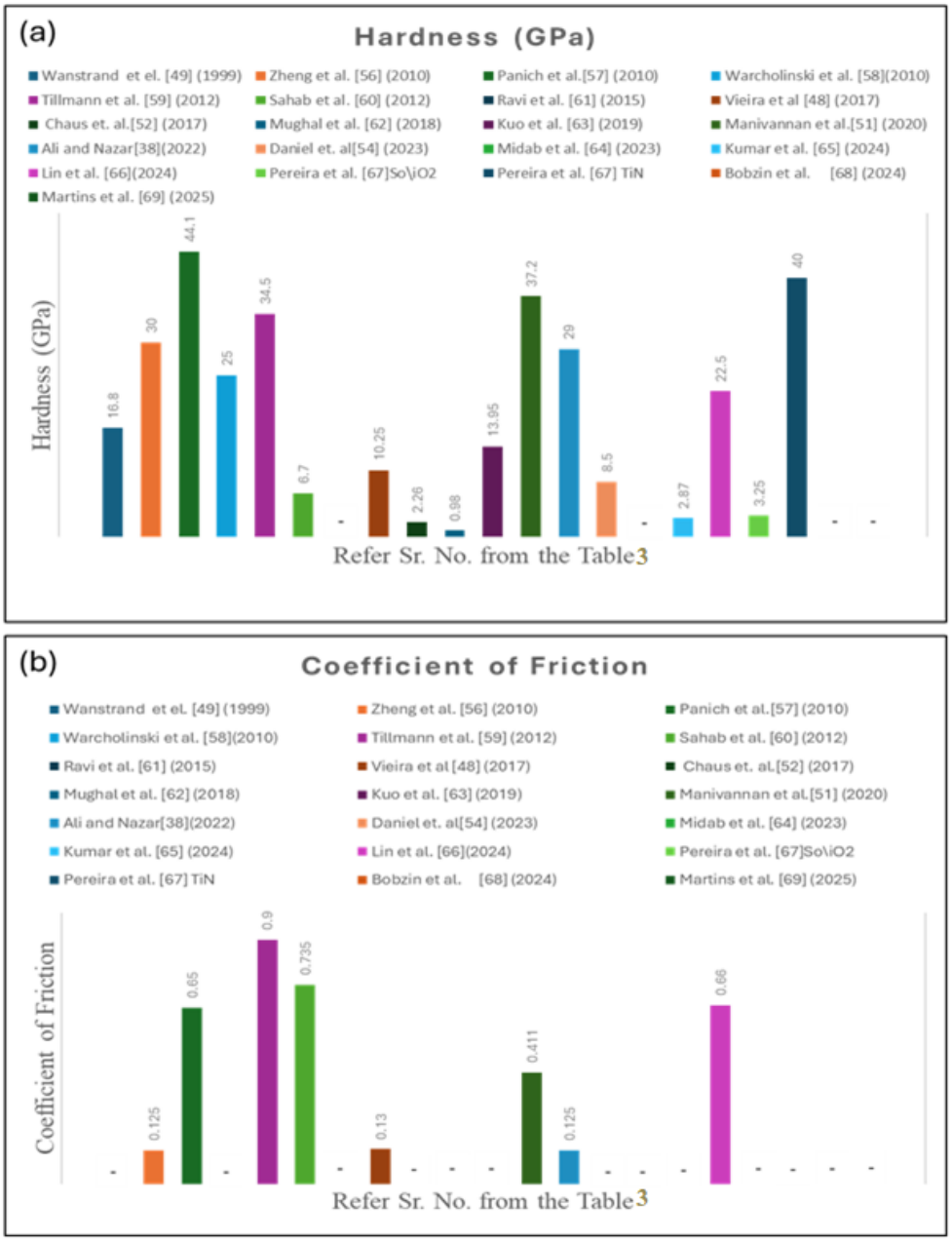

Fig. 10. A detailed comparison of the various ceramic coatings that have hardness and coefficient of friction based on the data mentioned in Table 2. The highest value of coating hardness was observed by Panich et al. [55] (2010), and Pereira et al. [67] (2024), which is around 44 and 40 GPa. The average coefficient of friction observed was 0.125 in case of CN_x/TiN by Zheng et al. [54] (2010).

3. Future Scope

The above analysis indicates that the research in ceramics coatings for HSS as a substrate for tribological and mechanical applications has been substantial, but there are still areas that have not so explored or require further research. These include as following:

a) Typically, the right elements and deposition conditions to achieve favorable tribological and mechanical properties are currently determined by hit-and-trial experiments and reviewing existing research, which offer a very slow and time-consuming process. So there is a need for soft computational modeling to achieve that target.

b) Research should focus on self-lubricating ceramic coatings on high-speed steel as a current area of focus to enhance tribological performance. there is a need for further investigation on this topic, considering the critical aspects, such as (i) cost analysis (ii) sustainability.

4. CONCLUSIONS

In this review paper, an attempt is made to present and discuss various ceramic protective coatings against mechanical and tribological properties, and conclude that:

(1) Different techniques were applied to high-speed steel, and their impact on wear resistance, friction, and hardness was evaluated.
(2) The properties of coatings also depended on the surface structure and morphology of the substrate.
(3) Adhesion of ceramic coatings to high-speed steel is vital for industries, especially cutting tools.
(4) Thermal spray coating yields superior tribological and mechanical results when compared to PVD and CVD, when combined with ceramic coatings for HSS, and high deposition rates of thermal spray coating also make them generally less expensive per unit area.
(5) Self-lubricating ceramic coatings, i.e. DLC coating, have demonstrated considerable enhancement in mechanical and tribological properties on various substrates, such as the HSS substrate. So self-lubricating coatings are the latest trending topic to explore for research advancements with benefits in cost-efficient and innovative approaches to minimize friction in machine tools.

REFERENCES

[1] G. Considerations, Cutting-tool Materials, (1997).
[2] J.-D. Kim, I. Zverv, K.-B. Lee, Thermal Model of High-Speed Spindle Units, Intell. Inf. Manag. 02 (2010) 306–315. https://doi.org/10.4236/iim.2010.25036.
[3] M. Boccalini, H. Goldenstein, Solidification of high speed steels, Int. Mater. Rev. 46 (2001) 92–115. https://doi.org/10.1179/095066001101528411.
[4] X. Tian, J. Zhao, J. Zhao, Z. Gong, Y. Dong, Effect of cutting speed on cutting forces and wear mechanisms in high-speed face milling of Inconel 718 with Sialon ceramic tools, Int. J. Adv. Manuf. Technol. 69 (2013) 2669–2678. https://doi.org/10.1007/s00170-013-5206-4.
[5] N.B. Dhokey, A. Hake, S. Kadu, I. Bhoskar, G.K. Dey, Influence of cryoprocessing on mechanism of carbide development in cobalt-bearing high-speed steel (M35), Metall. Mater. Trans. A Phys. Metall. Mater. Sci. 45 (2014) 1508–1516. https://doi.org/10.1007/s11661-013-2067-2.
[6] J.L. Mo, M.H. Zhu, B. Lei, Y.X. Leng, N. Huang, Comparison of tribological behaviours of AlCrN and TiAlN coatings-Deposited by physical vapor deposition, Wear 263 (2007) 1423–1429. https://doi.org/10.1016/j.wear.2007.01.051.
[7] M. Nalbant, H. Gökkaya, I. Toktaş, G. Sur, The experimental investigation of the effects of uncoated, PVD- and CVD-coated cemented carbide inserts and cutting parameters on surface roughness in CNC turning and its prediction using artificial neural networks, Robot. Comput. Integr. Manuf. 25 (2009) 211–223. https://doi.org/10.1016/j.rcim.2007.11.004.
[8] S.M. Lee, H.M. Chow, F.Y. Huang, B.H. Yan, Friction drilling of austenitic stainless steel by uncoated and PVD AlCrN- and TiAlN-coated tungsten carbide tools, Int. J. Mach. Tools Manuf. 49 (2009) 81–88. https://doi.org/10.1016/j.ijmachtools.2008.07.012.
[9] R.R.R. Malarvannan, T. V. Moorthy, P. Hariharan, P. Prabhu, Investigation on HSS single point cutting tool manufactured using physical vapor deposition coating process, Indian J. Eng. Mater. Sci. 23 (2016) 129–133.
[10] B. Fotovvati, N. Namdari, A. Dehghanghadikolaei, On coating techniques for surface protection: A review, J. Manuf. Mater. Process. 3 (2019). https://doi.org/10.3390/jmmp3010028.
[11] O. Id, C.O. Id, R. Relation, O. Information, R.D. Brown, A.M. Reviews, Handbook of tribology: materials, coatings, and surface treatments, Choice Rev. Online 29 (1992) 29-3326-29–3326. https://doi.org/10.5860/choice.29-3326.
[12] H. Cao, X.P. Dong, S. Chen, M. Dutka, Y. Pei, Microstructure evolutions of graded high-vanadium tool steel composite coating in-situ fabricated via atmospheric plasma beam alloying, J. Alloys Compd. 720 (2017) 169–181. https://doi.org/10.1016/j.jallcom.2017.05.226.
[13] P. Wang, W. He, G. Mauer, R. Mücke, R. Vaßen, Monte Carlo simulation of column growth in plasma spray physical vapor deposition process, Surf. Coatings Technol. 335 (2018) 188–197. https://doi.org/10.1016/j.surfcoat.2017.12.023.
[14] A.S. Chaus, L. Čaplovič, J. Porubský, Microstructure and properties of CBN diffusion coating on high-speed steel, Defect Diffus. Forum 312–315 (2011) 542–547. https://doi.org/10.4028/www.scientific.net/ DDF.312-315.542.
[15] H. Zhang, Y. Pan, Y.Z. He, Grain refinement and boundary misorientation transition by annealing in the laser rapid solidified 6FeNiCoCrAlTiSi multicomponent ferrous alloy coating, Surf. Coatings Technol. 205 (2011) 4068–4072. https://doi.org/10.1016/j.surfcoat.2011.02.054.
[16] K. Qi, Y. Yang, G. Hu, X. Lu, J. Li, Thermal expansion control of composite coatings on 42CrMo by laser cladding, Surf. Coatings Technol. 397 (2020) 125983. https://doi.org/10.1016/j.surfcoat.2020.125983.
[17] Y.L. Kuo, K.H. Chang, Atmospheric pressure plasma enhanced chemical vapor deposition of SiOx films for improved corrosion resistant properties of AZ31 magnesium alloys, Surf. Coatings Technol. 283 (2015) 194–200. https://doi.org/10.1016/j.surfcoat.2015.11.004.
[18] J.R. García, J.E. Fernández, J.M. Cuetos, F.G. Costales, Fatigue effect of WC coatings thermal sprayed by HVOF and laser treated, on medium carbon steel, Eng. Fail. Anal. 18 (2011) 1750–1760. https://doi. org/10.1016/j.engfailanal.2011.03.026.
[19] O.Y. Goncharov, I. V. Sapegina, R.R. Faizullin, L.K. Baldaev, Tantalum chemical vapour deposition on steel and tungsten substrates in the TaBr5-Cd-He system, Surf. Coatings Technol. 377 (2019) 124893. https://doi.org/10.1016/j.surfcoat.2019.124893.
[20] N.J. Archer, Advances in coating technology for tools., (1981).
[21] K. Bobzin, High-performance coatings for cutting tools, CIRP J. Manuf. Sci. Technol. 18 (2017) 1–9. https://doi.org/10.1016/j.cirpj.2016.11.004.
[22] L. Aissani, A. Alhussein, A.W. Zia, G. Mamba, S. Rtimi, Magnetron Sputtering of Transition Metal Nitride Thin Films for Environmental Remediation, Coatings 12 (2022) 1–29. https://doi.org/10.3390/ coatings12111746.
[23] A. Inspektor, P.A. Salvador, Architecture of PVD coatings for metalcutting applications: A review, Surf. Coatings Technol. 257 (2014) 138–153. https://doi.org/10.1016/j.surfcoat.2014.08.068.
[24] J. Decrozant-Triquenaux, L. Pelcastre, C. Courbon, B. Prakash, J. Hardell, High temperature tribological behaviour of PVD coated tool steel and aluminium under dry and lubricated conditions, Friction 9 (2021) 802–821.

https://doi.org/10.1007/s40544-020-0435-7.
[25] N. Schalk, M. Tkadletz, C. Mitterer, Hard coatings for cutting applications: Physical vs. chemical vapor deposition and future challenges for the coatings community, Surf. Coatings Technol. 429 (2022) 127949. https://doi.org/10.1016/j.surfcoat.2021.127949.
[26] B. Huang, C. Zhang, G. Zhang, H. Liao, Wear and corrosion resistant performance of thermal-sprayed Fe-based amorphous coatings: A review, Surf. Coatings Technol. 377 (2019) 124896. https://doi.org/10. 1016/j.surfcoat.2019.124896.
[27] A.K. Bisht, R.O. Vaishya, R.S. Walia, G. Singh, Nitrides ceramic coatings for tribological applications: A journey from binary to high-entropy compositions, Ceram. Int. 50 (2024) 8553–8585. https://doi.org/10. 1016/j.ceramint.2023.12.245.
[28] S. Dangi, R.S. Walia, N.M. Suri, S. Chaudhary, Tribological study on cast iron based, graphite and CNT enriched hybrid HVOF coating from room temperature to 300°C, Trans. Inst. Met. Finish. 0 (2023) 1–13. https://doi.org/10.1080/00202967.2023.2251756.
[29] A. Tyagi, R.S. Walia, Q. Murtaza, Tribological behavior of temperature dependent environment friendly thermal CVD diamond coating, Diam. Relat. Mater. 96 (2019) 148–159. https://doi.org/10.1016/ j.diamond.2019.05.003.
[30] A. Tyagi, R.S. Walia, Q. Murtaza, S.M. Pandey, P.K. Tyagi, B. Bajaj, A critical review of diamond like carbon coating for wear resistance applications, Int. J. Refract. Met. Hard Mater. 78 (2019) 107–122. https://doi.org/10.1016/j.ijrmhm.2018.09.006.
[31] C. Donnet, A. Erdemir, Historical developments and new trends in tribological and solid lubricant coatings, Surf. Coatings Technol. 180–181 (2004) 76–84. https://doi.org/10.1016/j.surfcoat.2003.10.022.
[32] H. Çalişkan, Selection of boron based tribological hard coatings using multi-criteria decision making methods, Mater. Des. 50 (2013) 742–749. https://doi.org/10.1016/j.matdes.2013.03.059.
[33] R. Rana, Q. Murtaza, R.S. Walia, Optimization using genetic algorithm of tribological behaviour of wc tool material, Indian J. Eng. Mater. Sci. 27 (2020) 889–896. https://doi.org/10.56042/ijems.v27i4.44867.
[34] K.R. Sharma, D. Das, Integrated Review of Thermo-Physical Properties of DifferentCeramic Coatings to make them Suitable for InternalCombustion Engines, 13 (2013). https://engineeringresearch.org/ index.php/GJRE/article/view/967/899.
[35] C. Fei, Z. Hai, C. Chen, X. Yangjian, Study on the tribological performance of ceramic coatings on titanium alloy surfaces obtained through microarc oxidation, Prog. Org. Coatings 64 (2009) 264–267. https://doi.org/10.1016/j.porgcoat.2008.08.034.
[36] Y. Jin, Y. Yang, Tribological behavior of various plasma-sprayed ceramic coatings, Surf. Coatings Technol. 88 (1997) 248–254. https://doi.org/10.1016/S0257-8972(96)02918-0.
[37] K. Holmberg, A. Matthews, H. Ronkainen, Coatings tribology - Contact mechanisms and surface design, Tribol. Int. 31 (1998) 107–120. https://doi.org/10.1016/S0301-679X(98)00013-9.F
[38] A. Ali, S.N. Ahmad, Mechanical and tribological behavior of TiB_2/Al_2O_3 coating on high-speed steel using electron beam deposition, Tribol. Int. 174 (2022) 107681. https://doi.org/10. 1016/j.triboint. 2022.107681.
[39] L. He, Y. Tan, X. Wang, T. Xu, X. Hong, Microstructure and wear properties of Al_2O_3-CeO_2 /Ni-base alloy composite coatings on aluminum alloys by plasma spray, Appl. Surf. Sci. 314 (2014) 760–767. https://doi.org/10.1016/j.apsusc.2014.07.047.
[40] Y. Lin, Y. Lei, H. Fu, J. Lin, Microstructure and Properties of (TiB_2 + NiTi)/Ti Composite Coating Fabricated by Laser Cladding, J. Mater. Eng. Perform. 24 (2015) 3717–3725. https://doi.org/10.1007/s11665-015-1668-x.
[41] N. Nedfors, S. Mráz, J. Palisaitis, P.O.Å. Persson, H. Lind, S. Kolozsvari, J.M. Schneider, J. Rosen, Influence of the Al concentration in Ti-Al-B coatings on microstructure and mechanical properties using combinatorial sputtering from a segmented TiB 2 /AlB 2 target, Surf. Coatings Technol. 364 (2019) 89–98. https://doi.org/10.1016/j.surfcoat.2019.02.060.
[42] W. Tillmann, A.L. Meijer, T. Platt, D. Biermann, D. Stangier, N.F. Lopes Dias, Cutting performance of TiAlN-based thin films in micromilling high-speed steel AISI M3:2, Manuf. Lett. 40 (2024) 6–10. https://doi.org/10.1016/j.mfglet.2024.01.005.
[43] V.F.C. Sousa, F.J.G. Da Silva, G.F. Pinto, A. Baptista, R. Alexandre, Characteristics and wear mechanisms of tialn-based coatings for machining applications: A comprehensive review, Metals (Basel). 11 (2021) 1–49. https://doi.org/10.3390/met11020260.
[44] K. Sarakinos, L. Martinu, Synthesis of thin films and coatings by high power impulse magnetron sputtering, Elsevier Inc., 2019. https://doi.org/10.1016/B978-0-12-812454-3.00013-9.
[45] Z. Hubička, J.T. Gudmundsson, P. Larsson, D. Lundin, Hardware and power management for high power impulse magnetron sputtering, 2019. https://doi.org/10.1016/B978-0-12-812454-3.00007-3.
[46] W. Tillmann, D. Stangier, D. Grisales, TiAlN-Beschichtungen mittels hoch-energetischer Kathodenzerstäubung: Eine Studie zur Auswirkung von Eigenspannungen auf die Leistungsfähigkeit von TiAlN-Dünnschichtsystemen, Vak. Forsch. Und Prax. 32 (2020) 26–32. https://doi.org/10.1002 /vipr.202000737.
[47] A.E. Özgür, B. Yalçin, M. Koru, Investigation of the wear performance and thermal diffusivity properties of M41 tools steel coated with various film coatings, Mater. Des. 30 (2009) 414–417. https://doi.org/10.1016/j.matdes.2008.05.020.
[48] D. Umbrello, L. Filice, S. Rizzuti, F. Micari, On the evaluation of the global heat transfer coefficient in cutting, Int. J. Mach. Tools Manuf. 47 (2007) 1738–1743. https://doi.org/10.1016/j.ijmachtools. 2006.12.002.
[49] V.F. Vieira, Y. Shigaki, P.S. Martins, E.C.T. Ba, C.A.R. Dias, Nanoindentation test of a DLC coated high-speed steel substrate using a two-dimensional axisymmetric finite element method, Diam. Relat. Mater. 134 (2023). https://doi.org/10.1016/j.diamond.2023.109792.
[50] A.S. Chaus, P. Pokorný, Čaplovič, M. V. Sitkevich, J. Peterka, Complex fine-scale diffusion coating formed at low temperature on high-speed steel substrate, Appl. Surf. Sci. 437 (2018) 257–270. https://doi.org/10.1016/j.apsusc.2017.12.173.
[51] L.M. Felix, The effect of Electro Spark Deposition on the microstructure and mechanical properties of IN718 by, (2018).
[52] K.W. Lee, Y.W. Chung, C. Korach, L.M. Keer, Tribological and dry machining evaluation of superhard TiB_2/ TiC multilayer coatings deposited on Si(001), M2 steel, and C3 WC cutting tool inserts using magnetron sputtering, Surf. Coatings Technol. 194 (2005) 184–189. https://doi.org/10.1016/ j.surfcoat.2004.10.124.
[53] O. Wänstrand, M. Larsson, P. Hedenqvist, Mechanical and tribological evaluation of PVD WC/C coatings, Surf. Coatings Technol. 111 (1999) 247–254. https://doi.org/10.1016/S0257-8972(98)00821-4.
[54] X.H. Zheng, J.P. Tu, R.G. Song, Fabrication, microstructure and tribological behavior of pulsed laser deposited a-CN_x/TiN multilayer films, Surf. Coatings Technol. 205 (2010) 902–908. https://doi.org/10.1016/j.surfcoat.2010.08.045.

[55] N. Panich, P. Wangyao, P. Visuttipitukul, S. Tungasmita, Y.K. Tan, Y. Sun, Mechanical and tribological behavior of nanostructured TIB2 coating on high speed steel, Int. J. Mod. Phys. B 24 (2010) 94–105. https://doi.org/10.1142/S0217979210064022.
[56] B. Warcholinski, A. Gilewicz, Z. Kuklinski, P. Myslinski, Hard CrCN/CrN multilayer coatings for tribological applications, Surf. Coatings Technol. 204 (2010) 2289–2293. https://doi.org/10. 1016/j.surfcoat.2009.12.019.
[57] W. Tillmann, G. Bejarano, F. Hoffmann, Deposition of hard and adherent TiBCN films for cutting tools applications, Phys. Status Solidi Appl. Mater. Sci. 209 (2012) 1520–1525. https://doi.org/10. 1002/pssa.201228130.
[58] A.R.M. Sahab, N.H. Saad, S. Kasolang, J. Saedon, Impact of plasma spray variables parameters on mechanical and wear behaviour of plasma sprayed Al_2O_3 3%wt TiO_2 coating in abrasion and erosion application, Procedia Eng. 41 (2012) 1689–1695. https://doi.org/10.1016/j.proeng.2012.07.369.
[59] N. Ravi, R. Markandeya, S. V. Joshi, Effect of substrate roughness on adhesion and tribological properties of nc-TiAlN/a-Si3N4 nanocomposite coatings deposited by cathodic arc PVD process, Surf. Eng. 33 (2017) 7–19. https://doi.org/10.1179/1743294415Y.0000000005.
[60] K. Mughal, M.Q. Saleem, M.P. Mughal, Performance evaluation of nano-composite ceramic-coated high-speed steel (HSS) drills in high-speed machining, Int. J. Adv. Manuf. Technol. 96 (2018) 4195–4203. https://doi.org/10.1007/s00170-018-1829-9.
[61] C.C. Kuo, Y.T. Lin, A. Chan, J.T. Chang, High temperature wear behavior of titanium nitride coating deposited using high power impulse magnetron sputtering, Coatings 9 (2019). https://doi.org/ 10.3390/coatings9090555.
[62] R. Manivannan, S. Sundararaj, R. Dheenasagar, K. Giridharan, P.R. Sivaraman, V. Udhayarani, Influence of Al2O3, SiC and B4C covalent multilayer PVD coating on surface properties of HSS rod, Mater. Today Proc. 39 (2020) 700–707. https://doi.org/10.1016/j.matpr.2020.09.225.
[63] J. Daniel, Š. Houdková, J. Duliškovič, J. Grossman, Impact wear of the Co-based HVOF-sprayed coatings, Tribol. Int. 187 (2023). https://doi.org/10.1016/j.triboint.2023.108755.
[64] W.A. Midab, H. Al-Ethari, S.J. Kareem, Improvement in Wear Resistance of the HSS Cutting Tool Surface by Ceramic Oxides Depositions, AIP Conf. Proc. 2830 (2023). https://doi.org/10.1063/5.0157225.
[65] N. Sathishkumar, G. Arumaikkannu, N. Thangapandian, E.A. Hem Anand, Exploring the impact of cryogenic treatment on detonation spray coated M2 high speed steel, Mater. Manuf. Process. 39 (2024) 2081–2098. https://doi.org/10.1080/10426914.2024.2394990.
[66] J. Lin, H. Luan, J. Li, J. Zhai, Y. Guan, G. Zhao, R. Bai, Enhanced Surface Mechanical and Tribological Properties of H13 Die Steel with TiAlSiN Coating Deposited by HiPIMS, Chinese J. Mech. Eng. (English Ed. 37 (2024). https://doi.org/10.1186/s10033-024-01128-z.
[67] N.F.S. Pereira, B.C.M. Reis, A.J. Dos Santos, M. Houmard, M.A. Câmara, A.R. Rodrigues, J.C.C. Rubio, Tribological assessment of the SiO2 coating deposited by sol–gel process toward cutting tool coating, Int. J. Adv. Manuf. Technol. 126 (2023) 487–503. https://doi.org/10.1007/s00170-023-11072-2.
[68] K. Bobzin, C. Kalscheuer, M. Tayyab, Tribological behavior of TiAlCrSiN coated cutting tools: Chip formation and friction analysis, Vak. Forsch. Und Prax. 36 (2024) 18–22. https://doi.org/10. 1002/vipr.202400817.
[69] P.S. Martins, R.M. Drumond, E.R. da Silva, E.C.T. Ba, P.M. Firpe, Comparison between the tribological aspects of AISI M-35 with and without diamond-like carbon coating, Wear 564–565 (2025). https://doi.org/10.1016/j.wear.2025.205733.